Recent and emerging applications of Graphene-based metamaterials in electromagnetics

Meisam Esfandiari [a], Ali Lalbakhsh [b,c,*], Paria Nasiri Shehni [a], Saughar Jarchi [a], Mohsen Ghaffari-Miab [d], Hamideh Noori Mahtaj [e], Sam Reisenfeld [b], Mohammad Alibakhshikenari [f], Slawomir Koziel [g,h], Stanislaw Szczepanski [h]

[a] Faculty of Engineering and Technology, Imam Khomeini International University (IKIU), Qazvin, Iran
[b] School of Engineering, Macquarie University, Sydney, Australia
[c] School of Electrical and Data Engineering, University of Technology Sydney (UTS), Sydney, NSW, Australia
[d] Faculty of Electrical and Computer Engineering, Tarbiat Modares University, Tehran, Iran
[e] Faculty of Electrical and Computer Engineering, Shahid Beheshti University, Tehran, Iran
[f] Department of Signal Theory and Communications, Universidad Carlos III de Madrid, Leganés, Madrid, 28911, Spain
[g] Department of Engineering, Reykjavik University, Reykjavik 102, Iceland
[h] Faculty of Electronics, Telecommunications and Informatics, Gdansk University of Technology, Gdansk 80-233, Poland

HIGHLIGHTS

- Graphene-based metasurfaces for reconfigurable antennas.
- Coupling reduction and orbital angular momentum using graphene-based metamaterials.
- Graphen-based plasmonic sensors for emerging applications.
- Electromagnetic graphene enabled absorbers.

GRAPHICAL ABSTRACT
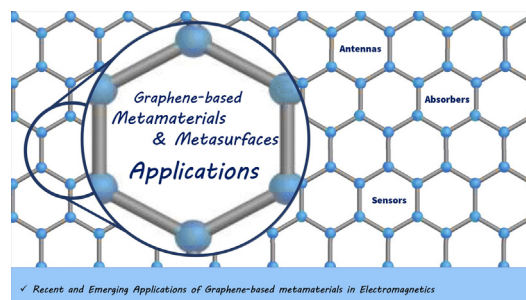
✓ Recent and Emerging Applications of Graphene-based metamaterials in Electromagnetics

ARTICLE INFO

ABSTRACT

Surface Plasmon Polaritons (SPPs) operating in mid-infrared up to terahertz (THz) frequencies have been traditionally manufactured on expensive metals such as gold, silver, etc. However, such metals have poor surface confinement that limits the optical applications of SPPs. The invention of graphene is a breakthrough in plasmon-based devices in terms of design, fabrication and applications, thanks to its plasmonic wave distribution, low-cost prototyping and its inherent reconfigurability. In addition, recent advancements in plasmon-based metamaterials and metasurfaces led to the elimination of the past constraints on regular optical devices, opening a new door in THz devices and applications. This paper provides an operational perspective of the advanced graphene-based electromagnetic devices, with a focus on graphene enabled antennas, absorbers and sensors, analyzing the strengths and limitations of various design methodologies.

* Corresponding author.
  E-mail address: ali.lalbakhsh@mq.edu.au (A. Lalbakhsh).

1. Introduction

The science of plasmonic has recently gained extensive attention due to its optical properties in metal and semiconductors [1–3]. Surface plasmonic resonance is a quantum-electromagnetic phenomenon produced by the interaction of light with free electrons at metal and a dielectric interface, resulting in

$$\sigma(w, \mu_c, \Gamma, T) = \frac{je^2(w - j2\Gamma)}{\pi\hbar^2}\left[\frac{1}{(w - j2\Gamma)^2}\int_0^{+\infty}\varepsilon\left(\frac{\partial f_d(\varepsilon)}{\partial\varepsilon} - \frac{\partial f_d(-\varepsilon)}{\partial\varepsilon}\right)d\varepsilon - \int_0^{+\infty}\varepsilon\left(\frac{\partial f_d(-\varepsilon) - \partial f_d(\varepsilon)}{(w - j2\Gamma)^2 - 4(\frac{\varepsilon}{\hbar})^2}\right)d\varepsilon\right], \tag{1}$$

longitudinal electromagnetic waves known as plasmonic waves [4–6]. In particular situations, the photon's energy is transferred into free electrons on the material surfaces which is called surface plasmon (SP). Two-dimension materials united with plasmonic nanostructures show a diversity of optical features, which contains efficient charge transfer, plasmonic hot-electron doping term, greater light spectrum emission, and very sensitive photodetection. Therefore, upcoming technologies offer a great opportunity to determine different photonic and optoelectronic utilizations of plasmonic nanostructures in combination with 2D materials [5].

There are numerous applications to this phenomenon that include biological application fields [7], chemistry [8], gaseous sensors [9], image sensors [10,11], and communication devices such as antennas [12]. Some metals like gold, silver, and copper can produce plasmonic waves in wavelengths lower than mid-infrared (mid-IR). However, there is a vast demand for surface plasmonic waves in mid-IR and terahertz bands [13–15] and [16–18].

Since the invention of graphene in 2004, it has been considered a promising material for designing plasmon-based devices without the need for metals, while it has brought a large degree of freedom in the design and functionality of plasmon-based devices [19–24]. In particular, graphene has unique electrical, optical, and chemical characteristics that metals do not possess that make it effective in plasmonic sensors, antennas and absorbers [25–27]. These features include high carrier mobility, photo response, broadband photodetection from the ultraviolet to THz spectrum regions, flexibility, low price, etc. [28]. Therefore, graphene is used for the renovation of most optical structures such as transistors [29], optical antennas [30], biosensors [31], polarizer [32–35], modulator [36–39], optical displays [40], absorbers [41,42], filters [43,44], and etc. However, the most significant characteristic of graphene is its reconfigurability. The graphene's surface current is configurable by applying a gate voltage [45,46]. This unique feature of graphene has made a breakthrough in metamaterials and metasurfaces design [45,47,48].

This paper presents a systematic review of the recent and ongoing advancements of graphene-based EM devices for THz applications. The organization of the article is as follow: Section II briefly overviews the graphene theory. Section III focuses on graphene enabled antenna reconfigurabilities in the aspects of operating frequencies, radiation patterns and polarizations. Section IV discusses modern absorber design procedures using graphene-based metamaterials. And Section V reviews the recent graphene-based plasmonic sensors and their emerging applications in virus detection.

2. Graphene theory

The optical characteristics of graphene generally depend on its careers, movements, and other electrical features in the mid-IR to the terahertz frequency band. The applied voltage could configure the electric carriers of graphene. The conductivity of graphene includes two parts $\sigma(w, \mu_c, \tau, T) = \sigma_{inter} + \sigma_{intra}$. In this formula, w is the radian frequency, μ_c is the chemical potential, τ is the relaxation time and T is the environment's temperature. The graphene's conductivity is derived from the Kubo formula [49]. Without considering the magnetic field, this formula could be represented as:

Where $f_d(\varepsilon)$ (Fermi distribution function) is expressed as: $f_d(\varepsilon) = (e^{(\frac{\varepsilon - \mu_c}{K_B T})} + 1)^{-1}$ and other parameters of formula (1) are: e is electron charge, h and $\hbar$ are respectively the normal and reduced Planck's constant and K_B is Boltzmann's constant. In addition, the relationship between μ_c (chemical potential) and n_s (carrier density) is expressed as follows [50]:

$$n_s = \frac{2}{\pi\hbar^2 V_F^2}\int_0^\infty \varepsilon[(f_d(\varepsilon) - f_d(\varepsilon + 2\mu_c)]d\varepsilon, \tag{2}$$

where V_F is the Fermi velocity. Changing the chemical potential results in varying graphene's conductivity versus frequency. For instance, when $\mu_c = 0eV$, the conductivity of graphene is nearly 1000 times less than the settings of $\mu_c = 1eV$ [50].

As before mentioned, the conductivity of graphene is divided into two parts of inter-band and intra-band. However, it can be mentioned that σ_{inera} is considered as graphene's conductivity for the low THz frequency regime as follows [51,52]:

$$\sigma_{intra} = \frac{2e^2 K_B T}{\pi\hbar^2}\cdot\frac{i}{w + i\tau^{-1}}[\text{Ln}(2\cosh(\frac{\mu_c}{K_B T}))], \tag{3}$$

In which the real part is involved in the absorption and dissipation of energy due to the presence of intra-band electrons. In addition, the graphene's chemical potential that is related to carrier density is as follows [52]:

$$\mu_c = E_f = \sqrt{\pi\hbar^2 v_f^2 n} \tag{4}$$

The surface plasmon dispersion relations for unlimited graphene between two dielectric layers with dielectric permittivities of $\varepsilon_r, \varepsilon_r^{/}$ and $\mu_r = \mu_r^{/} = 1$ are calculated (for TM mode) as below [53,54]:

$$\frac{\varepsilon_r}{\sqrt{K_{TM}^2 - \frac{\varepsilon_r w^2}{c^2}}} + \frac{\varepsilon_r^{/}}{\sqrt{K_{TM}^2 - \frac{\varepsilon_r^{/} w^2}{c^2}}} + \frac{i\sigma}{w\varepsilon_0} = 0 \tag{5}$$

$$\frac{W}{C} = K_0$$

The formula above becomes as follows if the graphene layer is floating in the air ($\varepsilon_r = \varepsilon_r^{/} = 1$) [53,54]:

$$K_{TE} = K_0\sqrt{1 - \left(\frac{2}{\sigma\eta_0}\right)^2}; \tag{6}$$

Where $\eta_0 = \sqrt{\mu_0/\varepsilon_0} = 377\Omega$ is the free space impedance. Furthermore, for TE mode:

$$K_{TE} = K_0 \sqrt{1 - \left(\frac{\sigma \eta_0}{2}\right)^2} \tag{7}$$

And the dielectric of graphene equation could result from considering the graphene thickness of Δ [55]:

$$\varepsilon_g = \varepsilon_0 + \frac{i\sigma}{w\Delta} \tag{8}$$

Graphene is modelled as an anisotropic layer by a thickness of 0.5 nm in the reference [55]. The graphene thickness in most applications is considered 3 to 10 nm. The dielectric definition model type is generally used when graphene has a thickness, and the surface current model type is employed when graphene is considered a two-dimensional structure. In general, 2D conductive surface model for graphene in the simulation of the device disclose its material performance completely and efficiently [56]. The most important challenge in manufacturing graphene-based devices is the multifaceted industrial techniques and the expensive production limiting graphene-based fabrications. Among several manufacturing approaches, Chemical Vapour Deposition (CVD) technology can effectively produce graphene on a large scale. However, this technique may reduce the quality of graphene, leading to worsening conductive characteristics of graphene for metasurface or metamaterial-graphene based structures. Recently, some modern developments and methods, such as Pulsed laser deposition (PLD), have been proposed to resolve this issue[57–59].

2.1. EM applications of Graphene-Based metamaterials and metasurfaces

Metamaterial and metasurface structures can improve the performance of electromagnetic waves across specific boundary conditions. Metamaterials are unconventional materials made around unique micro-and nanoscale arrays, allowing them to interact with light waves and other forms of energy typically not found in nature. For example, the negative index of refraction of light is the most important characteristic of metamaterials. Metasurfaces are a type of metamaterial structures made of separate parts arranged in 2D to eliminate wide range of losses and challenges in nanofabrications. New generations of metasurfaces taking advantage of graphene reconfigurability have been introduced and used in designing antennas, absorbers and sensors in THz band through a low-cost implementation. The following Sections reviews these three main applications of graphene-based metamaterials and metasurfaces.

3. Graphene-based antennas

Antennas play a critical role in communication and radar systems. Antennas' adjustability can ameliorate their functionality by adapting antennas with environmental conditions and providing additional levels of functionality for sending or receiving data. A number of devices can be used to adjust the functionality of antennas, such as switches (PIN diodes, FETs), variable reactive loading, structural changes, etc [60–62]. However, there are some drawbacks associated with these methods, such as high tuning speed in PIN diodes or a small dynamic range in variable reactive loading. Graphene can be used in conjunction with metamaterials and metasurfaces to provide reconfigurability in terms of bandwidth and center frequency, illumination direction, and polarization [63,64] and [65,66]. In addition to the use of graphene-based metamaterials in antenna configuration, these structures are also used for other applications such as generating orbital angular momentum waves.

3.1. Frequency reconfigurability

The greatest advantage of graphene-metamaterials integration is enabling a wide range of reconfigurability characteristics in graphene-based antennas. Xianjun Huang and et al. (2016) designed a reconfigurable antenna using graphene in the GHz band [67], where graphene was modelled as a 2D layer with a surface impedance (Rs) variable by chemical potential. This graphene array antenna has an insertion loss of −9.55 dB at 7.89 GHz for Rs = 2000 O. However, as the graphene's surface impedance changes to Rs = 100 O, the reflection becomes −1.1 dB. In [68], an array antenna was introduced using a right/left-handed feeding network. The presence of a graphene layer under this feeding network led to the reconfigurability of the antenna's operating frequency, where the variation of chemical potential between 0 and 0.2 eV controls the operating frequency. In addition, the chemical potential variation caused the antenna's gain to change. An array antenna based on graphene metamaterials fed by a circular horn antenna was designed in [69]. The negative values of ε_r and μ_r are achieved for different chemical potential values for the frequency range of 400 GHz to 620 GHz. The maximum gain of 22.6 dB was obtained in this article for a chemical potential of 0.4 eV. Another example of frequency alteration using graphene metamaterials was presented in [66], where a graphene-based array of split-ring resonators under the main antenna led to changing the resonance frequency.

3.2. Radiation patterns reconfigurability

Radiation patterns reconfigurability is becoming one of the most critical features of modern antennas, thanks to the emerging applications associated with IoT and non-geostationary satellite communications [70–74]. This feature is critically advantageous for increasing channel capacity [75]. Meisam Esfandiari and et al. (2018) designed a 2X2 MIMO antenna using an upper layer placed with space above the antenna shown in Fig. 1 a [76], rotating the antenna's pattern between 0 and 37 degrees Fig. 1 b. The capacity of the channel was calculated for different transmitted powers by designing a scenario Fig. 1 c. This achievement revealed that the channel capacity is increased by 47% when aligning the pattern along the direction of the minimum loss. In [77], a negative refractive index was achieved using graphene and metal. This metamaterial structure resulted in rotating the designed antenna's pattern between 0 and −27 degrees by changing the graphene's chemical potential. This design approach is an efficient technique for creating antennas with reconfigurable patterns. The use of metallic metamaterials over graphene layers resulted in an antenna pattern covering 360 degrees as discussed in [78,79], where adjusting the chemical potential from 0 eV to 0.5 eV, resulted in the graphene/gold-based unit cells achieving high transmission (ON state) and almost total reflection (OFF state) at two frequency ranges independently, resulting in the main antenna beam to steer. The main antennas are enclosed with six graphene/gold metamaterials screen parts.

Another example of using graphene metasurfaces in a leaky-wave antenna for adjusting its pattern is demonstrated in [80], where the periodic gaps are generated between graphene metasurfaces layers equivalent to a series of capacitors in illumination direction. This method has achieved a minimum beam steering angle of −29 degrees at 1 THz and a maximum angle of 75 degrees at 3.41THz. Apart from the above procedures for manipulating radiation patterns, a revolutionary generation of all-metal metasurfaces has recently been developed by Lalbakhsh and et al, with unparalleled electromagnetic characteristics, a breakthrough in antenna engineering [81].
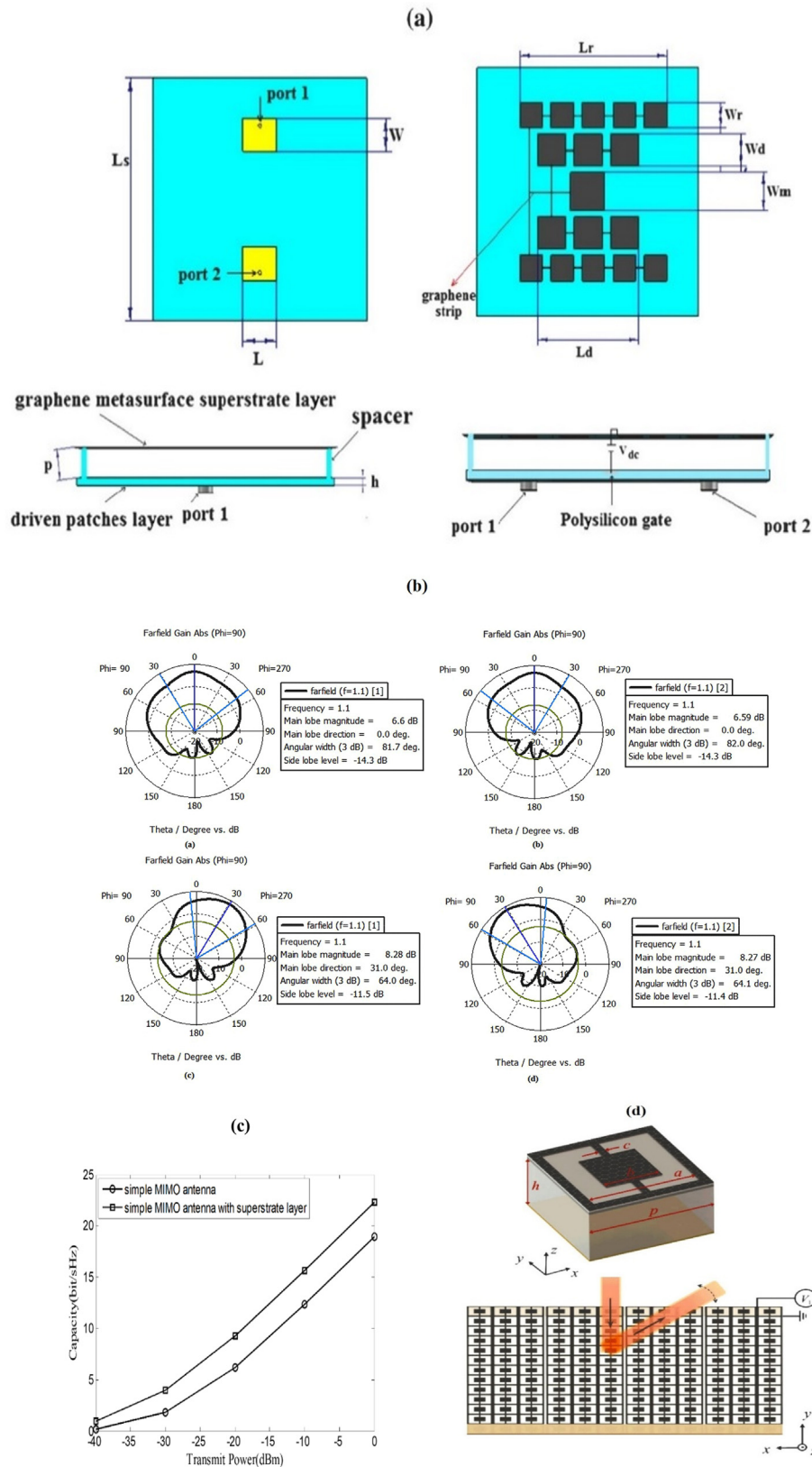
Fig. 1. (a) The geometry and sizes of the MIMO antenna (reproduced with permission from [76]). **(b)** Radiation pattern of the antenna with superstrate layer and μ_c = 0 eV for port 1, μ_c = 0 eV for port 2, μ_c= 1 eV for port 1, μ_c= 1 eV for port 2. **(c)** Channel capacity of the designed scenario with noise power of − 80 dBm. **(d)** Structure of the proposed metasurface and its unit cell (reproduced with permission from [84]).

3.3. Controlling antennas polarization

Graphene-based metamaterials have also been used for controlling antenna polarization [82]. Graphene-based metasurface was designed for converting linear to circular polarization [83]. The entire operating bandwidth of this polarization converter extends from 14 THz to 40 THz for the graphene chemical potential from 0.4 eV to 0.6 eV with ellipticity over 0.95. In [84], a graphene-based reconfigurable metasurface antenna scanning from 0 to 352.5 degrees at a terahertz band was presented with a maximum reflection at 46.5°. The average reflectivity of this design was 68.3%, and the maximum reflectivity variation range was only 30%. The structure of this antenna and its unit cell is shown in Fig. 1.d. The period boundary conditions need to be applied in the simulation when numerically calculating the scattering parameters of unitcells following the setting explained in [85,86]. To numerically calculate the frequency response of EM components, such as antennas, sensors, filters, couplers, absorbers, and photonic crystals, various computational approaches, including finite element, finite difference time-domain [87–90], finite-difference frequency-domain [91,92], are employed .

3.4. Coupling reduction and orbital angular momentum applications

Multi Input-Multi Output)MIMO(antennas play an essential role in increasing the capacity of the channels. However, the coupling between the components of the antenna is a significant challenge. Graphene-based structures have recently been considered as a promising solution to reduce the unwanted coupling in the MIMO antenna systems significantly.

Considerable coupling reduction was achieved in both GHz and THz frequency bands as reported in [93,94], and shown in Fig. 2, using graphene unit-cells. Another recent application of graphene is generating orbital angular momentum (OAM) waves [84,95–97]. OAM vortex waves can be generated by proper selection of chemical potential of graphene layers with modes 1, 2, and 3 in [95] and 0, 1, and 2 in [96], respectively. Both antennas cover a large frequency band of 1.8 ∼ 2.8 THz and 4.2 ∼ 5.6 THz, for references [95,96], respectively.

4. Graphene-based absorbers

Electromagnetic absorbers are engineering materials that can prevent the reflection and transmission of electromagnetic radiation. Electromagnetic absorbers have drawn increasing attention in many areas, such as designing selective thermal emitters, biosensors, photovoltaic devices, etc. Absorbers can be made of materials such as dielectrics combined with metal plates spaced at prescribed intervals or wavelengths. Over the last decade, metamaterials and metal-printed metasurfaces have played a significant role in designing EM absorbers. While this class of materials was only brought to EM absorber designs in early 2000, and is still considered a new approach, the introduction of graphene into the EM absorbers is opening a new chapter in EM absorber designs and applications [98–100]. Graphene is an appropriate alternative for expensive metals used in modern absorbers, such as gold and silver, thanks to its reconfigurability and its higher wave absorption rate [101,102]. This section discusses the recent graphene-based metamaterials design technologies for EM absorbers.

One of the critical characteristics of EM absorbers is their capability of handling EM waves with different polarizations. Water/graphene metamaterial was recently proposed to satisfy this requirement over a large frequency band [103]. This model demonstrates that the bandwidth of the absorber is increased by combining water with graphene-based metamaterial, as depicted in Fig. 3.

a. Water permittivity increases the bandwidth and coupled the absorption resonances. In this work, 90% absorption over a bandwidth of 4.5 THz was achieved around the central frequency of 6.77 THz at the room temperature of 300 Kelvin in the case of normal incidence. In the case of oblique incidence, the absorber maintains its 90% absorption up to 36 degrees over the bandwidth of 59% (4.66 THz to 8.61 THz). The characteristic curve of absorption for three different structures of A1, A2 and A12 for TE polarization and different chemical potentials are shown in Fig. 3.a. In [104], a graphene photodetector based on the metamaterial absorber in the visible and near-infrared bands was proposed. The investigational results indicate that the metamaterial-based graphene photodetector (MGPD) has attained up to 3751% of photocurrent. Moreover, the symmetric square-ring unit cell allows polarization-independent photo response at normal incidence. In [105–107], three structures of polarization an angle-insensitive graphene-based absorbers were developed. Under the oblique incidence, the absorptivity of the absorber is more than 90% over a wide range of incidence angles up to 60 degrees, 55 degrees for the TE and TM modes in [105,106], respectively. In addition, the results show 80% absorption for incident angles up to 45◦ for TE waves and up to 65◦ for TM waves were achieved [107].

Another graphene-based approach for maximizing absorption is the application of metallic metamaterial with graphene [108–110]. The combination of graphene and metallic metamaterials is the best means to attain active control of the electromagnetic wave. A C-shaped unit cell with a graphene layer under the cell, culminated in a maximum absorption in the range of 430 to 770 THz, the unit cell is shown in Fig. 1 b [111]. The purposed graphene-based metasurface absorber can be used as a basic building block of solar energy-harvesting photovoltaic devices. Additionally, the reflection of the absorber can be reduced by adding a bottom layer of tungsten. The absorption power is acquired using the following formulas:

$$\Delta \times \vec{E} = iw\mu_0 \vec{H}, \Delta \times \vec{H} = -iw\mu_0 \vec{E} \tag{9}$$

$$A(w) = \frac{Q_{abs}(w)}{Q_{inc}(w)} \tag{10}$$

$$Q_{abs} = \frac{w\varepsilon_0}{2} \int_v Im[\varepsilon(w)]|E|^2 dv \tag{11}$$

$$Q_{abs}^{tot} = \int A(w)F(w)dw \tag{12}$$

where Q_{abs}, $A(w)$, Q_{abs}^{tot} and $Q_{inc}(w)$ are spectral power absorbed by each section, optical absorption, total power absorbed and spectral power, respectively.

Greater absorption in the range of 99% can be achieved using square ring-shaped graphene-based metamaterials shown in Fig. 3 [112,113]. As shown in the absorption curves in Fig. 3d and Fig. 3e, there are three perfect absorption peaks in the terahertz band, corresponding to 25.53, 36.44 and 53.44 μm[112], and the absorption bandwidth is 2.88 GHz [113]. A dual bias is used for a single-layer graphene and a multi-layer absorber in [114]. The two most important features of this design are cost reduction and two-mode operation for the two biases. In the first mode, the absorption peaks occur at 4 THz and 5 THz, while the second mode shifted the peaks to the 6, 7 and 8 THz. Two sets of chemical potential values are recommended for a unique design for absorption at different frequencies.

Artificial intelligence (AI)-based approaches, such as genetic algorithms [115], particle swarm optimization [116–118], grey wolf optimization [119–122], neural network algorithms [123–132], and ant colony [133] have been recently brought to the EM
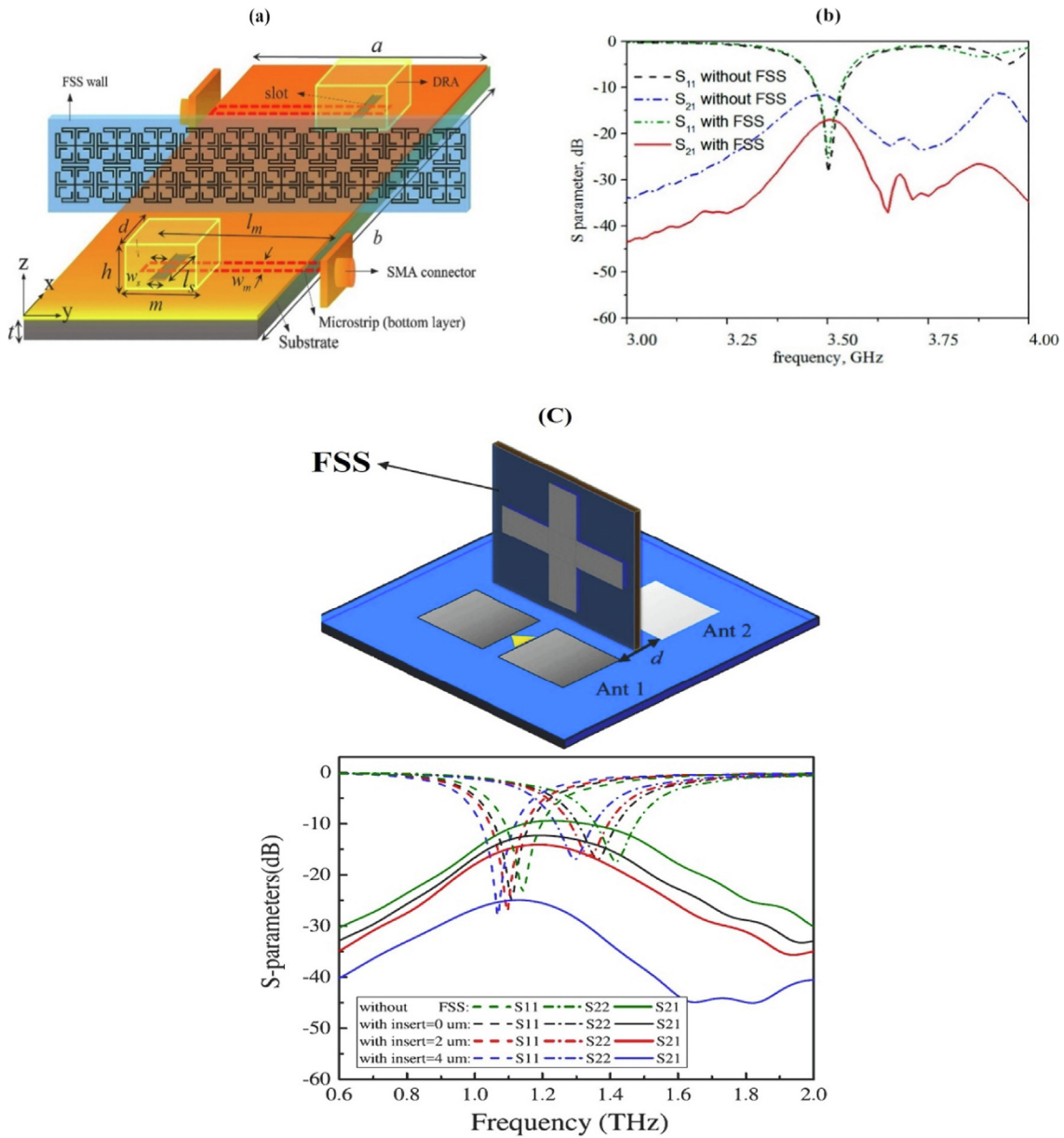
Fig. 2. (a) Geometric of MIMO antenna with FSS divider (reproduced with permission from [93]). **(b)** S-parameters responses for MIMO antenna with and without HCGF FSS divider (reproduced with permission from [93]). **(c)** The structure of the antennas, its FSS wall and S-parameter responses of the antennas model with and without separation (reproduced with permission from [94]).

community and also utilized in designing a wide range of EM components including graphene-based absorbers. For example, genetic algorithm was used to design a unit cell with graphene ribbons for reflection minimization, acquiring a 98% absorption ratio in the frequency band of 6.45 THz and 7.35 THz [101,134]. Further information on the aabove nature-based optimization can be found in [135].In this AI-based absorber, two periodic arrays of graphene ribbons and one graphene continuous sheet act as a coupling element to improve the absorption bandwidth. Genetic algorithms have also been used in reconfigurable graphene-based absorbers. In [136], dual bias method combined with the inherent graphene reconfigurability resulted in three modes that were then optimized by a genetic algorithm. In detail, manipulating the nano graphene disks increases the bias gates, enabling three reconfigurable modes of 0.7–2.3 THz, 5.3–6.6 THz, and 7.4–8.4 THz with an absorption rate higher than 90%. The configuration of some graphene-based metamaterial absorbers and their absorption bands are demonstrated in Table.1.

Absorbers applications have also been brought to sensing practices where a higher absorption rate increases sensitivity in plasmonic sensors. Consequently, the graphene-based absorbers have earned a special place in sensing applications [137,138]. In the following section, the graphene-based plasmonic sensors are discussed in detail.

5. Plasmonic sensors

The propagation of viruses has developed a threat to worldwide biosecurity, typified by the current COVID-19 pandemic. Accordingly, the investigation into epidemiologic infection and virus control has always been vital in these circumstances [139–141]. Recently, propagating surface plasmon resonance (SPR) has been used in plasmonic sensor design for virus detection [142–144].

The optical properties of materials led to encouraging applications in sensor fabrication. However, the time and confinement
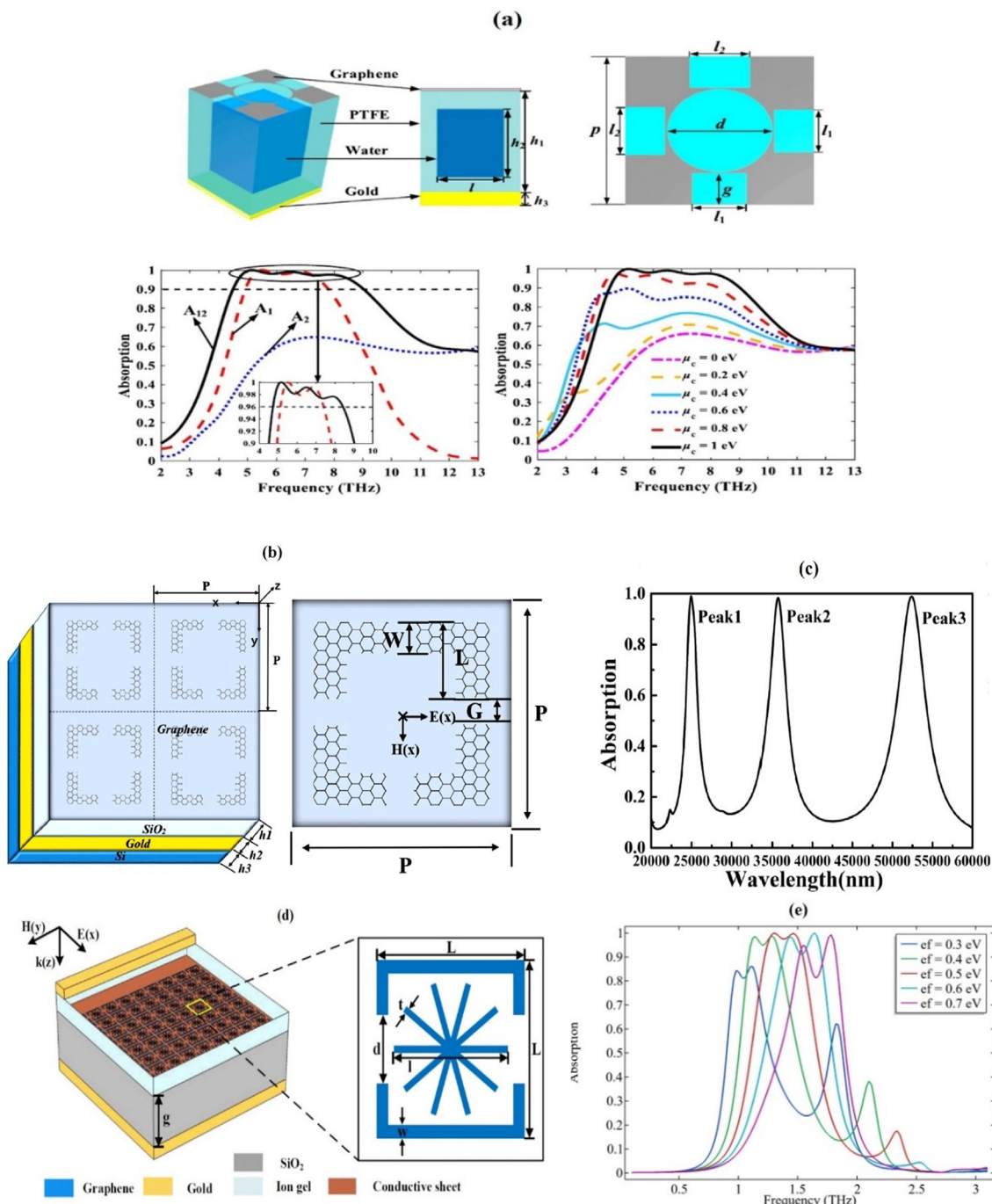
Fig. 3. (a) The schematic design of the absorber with 3D and top views and Simulated absorption spectra of absorber(reproduced with permission from [103]). **(b)** The diagram of a periodic array of graphene metamaterial absorber(reproduced with permission from [112]). **(c)** The absorption rate curve (reproduced with permission from [112]). **(d)** Geometric and unit cell structure of absorber (reproduced with permission from [113]). **(e)** Absorption bands for different chemical potentials(reproduced with permission from [113]).

capacity of such (SPPs) are very small in noble metals such as gold and Au. In addition, the Discovery and control of harmful and poisonous chemical materials, gases, micro-organisms and electromagnetic radiation has been a challenge for scientists to recover human and environmental health. 2D material-based sensors are very efficient and fit with new production technology, used for health and environment checking [145–147]. Graphene and Graphene-oxides, black phosphorus (BP), transition metal chalcogenides (TMDCs), metal oxides and other 2D nanomaterials are now considered attractive approaches for the manufacture of

highly sensitive sensors [148–151]. The invention of graphene and its plasmonic has opened a new door to designing SPR sensors. Surface plasmon polaritons (SPPs) can be produced in graphene at frequencies in the mid-infrared to terahertz range, which is not possible using conventional plasmonic materials such as noble metals. One of the most important property of graphene that distinguishes it from other two-dimensional materials is its adjustability by applying a voltage bias without changing the structure. This ability allows us to change the properties of the structure without changing its physical parameters. Close and conformal

Table 1
summary of graphene-based metamaterial absorbers.

Absorber Configuration	Absorption band	Reference
Graphene square ring-shaped	Triple bands, 25.33 μm,36.44 μm, 53.44 μm	[112]
Graphene split-ring nested with a cross line	Multi bands, between 3 THz to 11 THz	[138]
Graphene double-open rectangular ring with strip cross structure	Wideband, from 1.260 to 1.548 THz	[113]
Metal-based C-shaped metamaterial with monolayer graphene	Wideband, from 430 to 770 THz	[111]
Metal-based Minkowski -shaped with monolayer graphene	Multi bands, between 1200 nm and 1600 nm	[109]
Graphene ribbon	Wideband, from 6.45 THz to 7.35 THz	[134]
Graphene hallow-out squares	Wideband, from 1.14 THz to 3.31 THz	[101]
Water-graphene structure	Wideband, bandwidth of 4.50 THz	[103]

Fig. 4. The unit cell of the structure and simulated transmission amplitude curve (). reproduced with permission from [169]

interaction with tissues in the body, skin, brain and eyes is achievable by graphene-based sensors because of their flexible mechanic and their very thin thickness, which is necessary for attaining high-quality signals. On the other hand, graphene's high optical transparency and electrical conductivity make it a perfect material for bio-tissue investigations with good resolution images and without visual disturbances. Additionally, a high signal-to-noise ratio (SNR) in electrophysiological data signals can be achieved thanks to the excellent electrical conductivity of graphene [152–155]. The conscious, flexible chemistry of graphene-based nanomaterials, including the ability to intermix with water-soluble and water-insoluble active composites, proteins, DNA, cells and more other things creates them a favorite for modern bio-technologic with nano platform usages[156–159].

Moreover, combining graphene and metamaterials can achieve an ultrathin optical SPR sensor of high performance [25,160,161]. Regarding the performance of these sensor models, a resonant wavelength occurs in the reflection characteristic curve when the wave vector of the decaying waves and the wave vector of the surface plasmons are equal, where electrons or photons generate the surface plasmon polaritons. However, this generation requires a prism, a grating, a defect on the metal surface, or an optical fibre [20,162–164]. One the great advantages of graphene in manufacturing sensors are its high electrical and thermal conductivities and high control on functionalization. However, hydrophobicity, high cost, and production difficulties are considered its disadvantages [156].

Generally, there are two approaches for the analysis and investigation of plasmonic sensors; angle method and wavelength method [5]. Sensitivity (S), detection accuracy (D.A) and quality factor (Q) are three main parameters determining the performance of a sensor that are expressed as: $s = \frac{\sigma\lambda_{res}}{\sigma n_s}$. If the refractive index of the sensing layer differs by σn_s, the wavelength of the sensor differs by $\sigma\lambda_{res}$ in the output power, reflection or in the transmission curve. $D.A = \frac{\sigma\lambda_{res}}{\sigma\lambda_{0.5}}$ is the signal to noise ratio (D.A), can be determined by the output power characteristic curve. In addition, the sensitivity and the spectral width of the SPR curve are used to determine the quality factor of the sensor $Q = \frac{S}{\sigma\lambda_{0.5}}$ [20,165–167].

The following summarizes recent studies on plasmonic sensors using metal/graphene, graphene metamaterials and metasurfaces.

In 2014 a reconfigurable plasmonic sensor was designed based on two concentric graphene rings sandwiched between the sensitive region and the substrate [168]. This sensor demonstrated a sensitivity of 9.59 $\mu m/RIU$ for n = 1.4 and n = 1.5 in the best case. As stated in the last part of the absorbers section, graphene metamaterials increased absorption and sensitivity. In addition, the
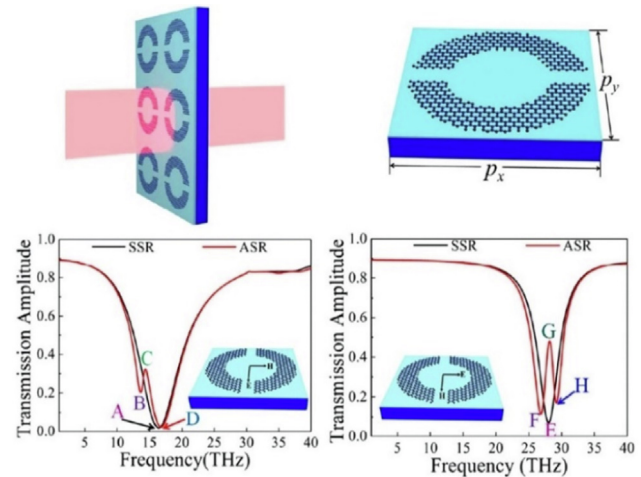
high degree of structural symmetry confirms that the sensor's spectral response is angle and polarization-independent. Moreover, the operating frequency of the sensing range can be tuned by doping chemical potential.

A resonator with a modulation depth of frequency and amplitude was proposed in [166,169], achieving 58.58% and 99.35%, 59.53% and 97.7% in the two crossed-polarization orientations. The structure and its transmission characteristic curve are shown in Fig. 4. When the chemical potential is 0.5 eV, the transmission characteristic curve is calculated for E field orientation (perpendicular and parallel to the gap of the unit cell) as shown in Fig. 4. When the electric polarization is oriented perpendicular to the two gaps, the (SSR) structure, the left and right arcs are with the same length, demonstrates only a single broad resonance at 16.39 THz; meanwhile, there are two resonances in ASR structure, one of them is at 16.71 THz and another with enormously sharp asymmetric resonance is at 13.66 THz. Also, there are two resonances at 26.84 THz and 29.22 THz when the electric polarization is oriented parallel to the two gaps in the ASR structure and one resonant dip in the SSR structure at 28.03 THz.

In [170], a multi-channel structural sensor with a detection limit of 10 pM for DNA was investigated. A single layer graphene/crystal was spotted into several channels to measure time and concentration of DNA hybridization kinetics and affinity consistently with high sensitivity, shown in Fig. 5. Cost-effective, high-throughput screening of drug candidates, genetic variations, and disease biomarkers are some of the most critical features of this sensor, opening a new research avenue in biosensing.
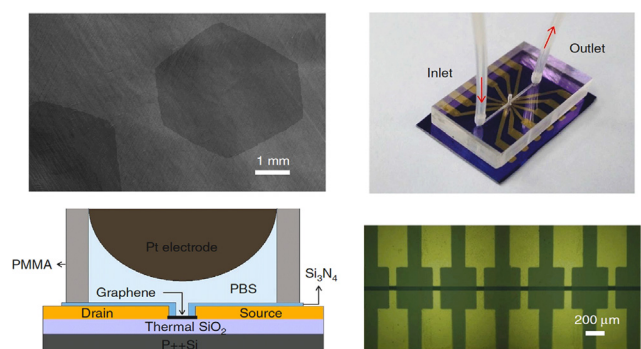

Fig. 5. View of the mentioned sensor composed of (multi-G-FETs) with a microfluidic channel along with solution inlet and outlet as labelled and its cross-sectional view (). reproduced with permission from [170]

Table 2
Summary of graphene-based metamaterial sensors.

Sensor Configuration	Application	FOM, Sensitivity	Reference
Graphene Elliptical ring	Biosensing, Environmental monitoring	, 14110 nm/RIU	[164]
Graphene disk with a SRR in unitcell	Nanoscale optical sensing	29, 28 cm^{-1}/RIU	[160]
Graphene-based narrowband	Selective sensing	277.8, 1.84 THz/RIU	[179]
Graphene split ring with T-stub (Two peaks)	*Medical diagnosing, Biosensing, environmental monitoring*	(10.8, 3.2), (5.6 μM/RIU, 17.2 μM/RIU)	[166]
Graphene Semi elliptical nano disk	Gas Sensing	3.9, 11.5 μM/RIU	[175]
Graphene nano disk	Multi substance detection	20.4, 550 cm^{-1}/RIU	[176]
FLU/graphene-based disk	For exciting surface plasmons	5.1, 1140 nm/RIU	[178]
Graphene concentering double rings	Gas sensing	5.82, 9.59 μM/RIU	[168]
Graphene-layered metamaterial	Nano sensing	9786, 7885 nm/RIU	[180]

Fig. 6. View of the (PIT-sensor) and its transmission curve for voltages of v_1 and v_2(). reproduced with permission from [172]

In [171], Wendao Xu et al. developed a hybrid golden/graphene-based metamaterial biosensor capable of decreasing down to 2 ng chlorpyrifos. The configuration of some graphene-based metamaterial sensors and their application, sensitivity and FOM are shown in Table.2. A sensor using two sets of micro-ribbon graphene was devised in Fig. 6. [172]. The plasmonic interaction between two ribbons increased the induced plasmons and, as a result, intensified the sensitivity. The results proved the exact sensing of benzoic acid with a detection limit smaller than 6.35 $\mu g/cm^2$. Enhancing the sensitivity can be an exciting feature for the PIT sensors for biochemical sensing. In [173], a Fano resonance sensor was achieved with a maximal sensitivity of 7885 nm/RIU.

Islam and et al. (2019) developed a multiband terahertz sensor and applied a genetic algorithm to optimize its performance [174], where a graphene layer for easing absorption was used. Additionally, an array of graphene-based metasurface was employed at the top layer to produce a greater evanescent wave. The main characteristic of this sensor was a 99.7% absorption in its operating bands suitable for sensing applications. Moreover, in [175,176], dual-band sensors were designed to achieve 11.5 and 550 1/cm.RIU sensitivities at their optimal performance. Their FOMs were 3.9 and 20.4, respectively, where the sensor in [175] was capable of handling incident angles of 0 to 60 degrees.

A graphene/dielectric periodic sensor with anisotropic distribution properties of hyperbolic metamaterials was developed in [177]. When the chemical potential of graphene increases over a certain value, the equifrequency contour of the sensor will transit from an ellipse to a hyperbola. In [178], a graphene-based tunable metasurface sensor was numerically analyzed, showing the excited plasmons attained a significant tunability with maximum sensitivity and FOM of 1140 nm/RIU and 5.1, respectively.

Xuemei Du and et al. (2021) introduced a dual-band absorber with excellent absorption, which enhances the structure's sensitivity. The results demonstrated that the sensor has a high Q-factor of 277.8 at 1.945 THz and the sensitivity reaches up to 1.84 THz/RIU [179]. A graphene-based elliptical ring unit-cell was introduced in [180,181], showing a sensitivity of 14110 nm/RIU and 21.1 $\mu m/RIU$ at their optimal performance, respectively.

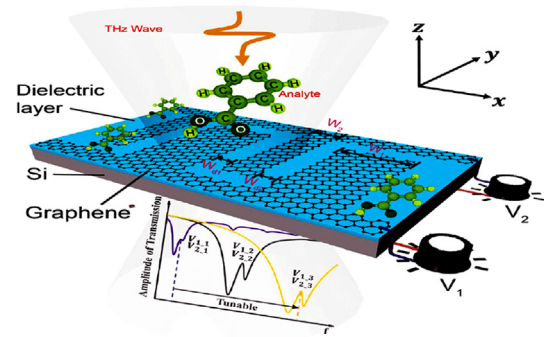In terms of the future perspective, the recent advancement in graphene-based metasurfaces is revolutionizing the field of pho-tonics in the terahertz (THz) frequency range. Antenna-sensors made of graphene have received significant attention with the Internet of Things (IoT) development and the ever-increasing popularity of wearable electronic devices. Electronic skin devices, implantable medical components and human health checking are the most critical applications of antenna sensors. Additionally, graphene-based metasurfaces can be used to structure reflect-array antennas.

6. Conclusion

Since 2004 Graphene has been introduced to electromagnetics engineering and revolutionized EM components in performance and versatility. Graphene-based metamaterials have unconventional photonic, electronic, thermal, and mechanical properties, allowing a great degree of freedom in THz operating devices. This article provides a comprehensive review of the recent advancements in electromagnetic engineering based on the newly introduced graphene and metal/graphene-based metamaterials to design modern antennas, absorbers and sensors.

Data availability

No data was used for the research described in the article.

Declaration of Competing Interest

The authors declare that they have no known competing financial interests or personal relationships that could have appeared to influence the work reported in this paper.

Acknowledgment

References

[1] D.K. Gramotnev, S.I. Bozhevolnyi, Plasmonics beyond the diffraction limit, Nat. Photonics 4 (2010) 83–91.
[2] S. Kawata, Plasmonics: Future Outlook, Jpn. J. Appl. Phys. 52 (2013) 010001.
[3] C. Genet, T.W. Ebbesen, "Light in tiny holes," (in eng), Nature 445 (7123) (2007) 39–46, https://doi.org/10.1038/nature05350.
[4] R. Harris, J.S. Wilkinson, Waveguide surface plasmon resonance sensors, Sens. Actuators, B 29 (1–3) (1995) 261–267.
[5] J. Homola, On the sensitivity of surface plasmon resonance sensors with spectral interrogation, Sens. Actuators, B 41 (1–3) (1997) 207–211.
[6] Z. Salamon, H.A. Macleod, G. Tollin, Coupled plasmon-waveguide resonators: a new spectroscopic tool for probing proteolipid film structure and properties, Biophys. J . 73 (5) (1997) 2791–2797.

[7] J.N. Anker, W.P. Hall, O. Lyandres, N.C. Shah, J. Zhao, R. p., Van Duyne, "Biosensing with plasmonic nanosensors,", Nanoscience and Technology: A Collection of Reviews from Nature Journals (2010) 308–319.

[8] C. Valsecchi, A.G. Brolo, Periodic metallic nanostructures as plasmonic chemical sensors, Langmuir 29 (19) (2013) 5638–5649.

[9] J. Qin, Y.-H. Chen, B. Ding, R.J. Blaikie, M. Qiu, Efficient plasmonic gas sensing based on cavity-coupled metallic nanoparticles, The Journal of Physical Chemistry C 121 (44) (2017) 24740–24744.

[10] S. Ogawa and M. Kimata, "Wavelength- or Polarization-Selective Thermal Infrared Detectors for Multi-Color or Polarimetric Imaging Using Plasmonics and Metamaterials," Materials, vol. 10, no. 5, p. 493, 2017. [Online]. Available: https://www.mdpi.com/1996-1944/10/5/493.

[11] Y. Kanamori, D. Ema, and K. Hane, "Miniature Spectroscopes with Two-Dimensional Guided-Mode Resonant Metal Grating Filters Integrated on a Photodiode Array," vol. 11, no. 10, p. 1924, 2018. [Online]. Available: https://www.mdpi.com/1996-1944/11/10/1924.

[12] Y. Tsur, I. Epstein, R. Remez, A. Arie, Wavefront shaping of plasmonic beams by selective coupling, ACS Photonics 4 (6) (2017) 1339–1343.

[13] J. Pendry, L. Martin-Moreno, F. Garcia-Vidal, Mimicking surface plasmons with structured surfaces, Science 305 (5685) (2004) 847–848.

[14] R. Stanley, Plasmonics in the mid-infrared, Nat. Photonics 6 (7) (2012) 409–411.

[15] Z. Gao, L. Wu, F. Gao, Y. Luo, B. Zhang, Spoof plasmonics: from metamaterial concept to topological description, Adv. Mater. 30 (31) (2018) 1706683.

[16] T. Lv et al., Hybrid metamaterial switching for manipulating chirality based on VO2 phase transition, Sci. Rep. 6 (1) (2016) 1–9.

[17] J. Shi et al., THz photonics in two dimensional materials and metamaterials: properties, devices and prospects, J. Mater. Chem. C 6 (6) (2018) 1291–1306.

[18] Y. Xiang, X. Dai, J. Guo, H. Zhang, S. Wen, D. Tang, Critical coupling with graphene-based hyperbolic metamaterials, Sci. Rep. 4 (1) (2014) 1–7.

[19] K.S. Novoselov et al., Two-dimensional gas of massless Dirac fermions in graphene, Nature 438 (7065) (2005) 197–200.

[20] M. Esfandiyari, M. Norouzi, P. Haghdoust, S. Jarchi, Study of a Surface Plasmon Resonance Optical Fiber Sensor Based on Periodically Grating and Graphene, Silicon 10 (6) (2018) 2711–2716, https://doi.org/10.1007/s12633-018-9810-7.

[21] M. Esfandiari, S. Jarchi, P. Nasiri-Shehni, M. Ghaffari-Miab, Enhancing the sensitivity of a transmissive graphene-based plasmonic biosensor, Appl. Opt. 60 (5) (2021) 1201–1208.

[22] P.-Y. Chen, C. Argyropoulos, M. Farhat, J.S. Gomez-Diaz, Flatland plasmonics and nanophotonics based on graphene and beyond, Nanophotonics 6 (6) (2017) 1239–1262.

[23] J. Zhang, W. Zhu, Graphene-Based Microwave Metasurfaces and Radio-Frequency Devices, Advanced Photonics Research 2 (11) (2021) 2100142.

[24] T. Guo, C. Argyropoulos, Recent advances in terahertz photonic technologies based on graphene and their applications, Advanced Photonics Research 2 (6) (2021) 2000168.

[25] Z. Vafapour, Y. Hajati, M. Hajati, H. Ghahraloud, Graphene-based mid-infrared biosensor, JOSA B 34 (12) (2017) 2586–2592.

[26] A. Andryieuski, A.V. Lavrinenko, Graphene metamaterials based tunable terahertz absorber: effective surface conductivity approach, Opt. Express 21 (7) (2013) 9144–9155.

[27] R. Bala, A. Marwaha, Development of computational model for tunable characteristics of graphene based triangular patch antenna in THz regime, J. Comput. Electron. 15 (1) (2016) 222–227, https://doi.org/10.1007/s10825-015-0761-6.

[28] J.H. Warner, F. Schaffel, M. Rummeli, A. Bachmatiuk, Graphene: Fundamentals and emergent applications, Newnes, 2012.

[29] F. Xia, D.B. Farmer, Y.-M. Lin, P. Avouris, Graphene field-effect transistors with high on/off current ratio and large transport band gap at room temperature, Nano Lett. 10 (2) (2010) 715–718.

[30] I. Llatser, C. Kremers, A. Cabellos-Aparicio, J.M. Jornet, E. Alarcón, D.N. Chigrin, Graphene-based nano-patch antenna for terahertz radiation, Photonics and Nanostructures-Fundamentals and Applications 10 (4) (2012) 353–358.

[31] S. Afsahi et al., Novel graphene-based biosensor for early detection of Zika virus infection, Biosens. Bioelectron. 100 (2018) 85–88.

[32] W. Yuan, G. Shi, Graphene-based gas sensors, J. Mater. Chem. A 1 (35) (2013) 10078–10091.

[33] T. Guo, C. Argyropoulos, Broadband polarizers based on graphene metasurfaces, Opt. Lett. 41 (23) (2016) 5592–5595.

[34] R.E. de Oliveira, C.J. de Matos, Graphene based waveguide polarizers: in-depth physical analysis and relevant parameters, Sci. Rep. 5 (1) (2015) 1–8.

[35] V. Sorathiya et al., Numerical investigation of the tunable polarizer using gold array and graphene metamaterial structure for an infrared frequency range, Appl. Phys. B 128 (1) (2022) 1–9.

[36] M. Pumera, Graphene-based nanomaterials for energy storage, Energy Environ. Sci. 4 (3) (2011) 668–674.

[37] K. Fan, J. Suen, X. Wu, W.J. Padilla, Graphene metamaterial modulator for free-space thermal radiation, Opt. Express 24 (22) (2016) 25189–25201.

[38] Z. Huang, Q. Han, C. Ji, J. Wang, Y. Jiang, Broadband terahertz modulator based on graphene metamaterials, AIP Adv. 8 (3) (2018) 035304.

[39] C. Argyropoulos, Enhanced transmission modulation based on dielectric metasurfaces loaded with graphene, Opt. Express 23 (18) (2015) 23787–23797.

[40] J.-H. Ahn, B.H. Hong, Graphene for displays that bend, Nat. Nanotechnol. 9 (10) (2014) 737–738, https://doi.org/10.1038/nnano.2014.226.

[41] Y. Cai, J. Zhu, Q.H. Liu, Tunable enhanced optical absorption of graphene using plasmonic perfect absorbers, Appl. Phys. Lett. 106 (4) (2015) 043105.

[42] M. Grande et al., Graphene-based perfect optical absorbers harnessing guided mode resonances, Opt. Express 23 (16) (2015) 21032–21042.

[43] V. Karpan et al., Graphite and graphene as perfect spin filters, Phys. Rev. Lett. 99 (17) (2007) 176602.

[44] H.-J. Li, L.-L. Wang, J.-Q. Liu, Z.-R. Huang, B. Sun, X. Zhai, Investigation of the graphene based planar plasmonic filters, Appl. Phys. Lett. 103 (21) (2013) 211104.

[45] L. Ju et al., Graphene plasmonics for tunable terahertz metamaterials, Nat. Nanotechnol. 6 (10) (2011) 630–634.

[46] J. Niu, Y. Jun Shin, Y. Lee, J.-H. Ahn, H. Yang, Graphene induced tunability of the surface plasmon resonance, Appl. Phys. Lett. 100 (6) (2012) 061116.

[47] P.Q. Liu et al., Highly tunable hybrid metamaterials employing split-ring resonators strongly coupled to graphene surface plasmons, Nat. Commun. 6 (1) (2015) 1–7.

[48] X. He, Tunable terahertz graphene metamaterials, Carbon 82 (2015) 229–237.

[49] V. Gusynin, S. Sharapov, J. Carbotte, Magneto-optical conductivity in graphene, J. Phys.: Condens. Matter 19 (2) (2006) 026222.

[50] G.W. Hanson, Dyadic Green's functions and guided surface waves for a surface conductivity model of graphene, J. Appl. Phys. 103 (6) (2008) 064302.

[51] L. Falkovsky, S. Pershoguba, Optical far-infrared properties of a graphene monolayer and multilayer, Physical Review B 76 (15) (2007) 153410.

[52] P.A.D. Gonçalves, N.M. Peres, An introduction to graphene plasmonics, World Scientific, 2016.

[53] S.A. Mikhailov, K. Ziegler, New electromagnetic mode in graphene, Phys. Rev. Lett. 99 (1) (2007) 016803.

[54] X.Y. He, R. Li, Comparison of graphene-based transverse magnetic and electric surface plasmon modes, IEEE J. Sel. Top. Quantum Electron. 20 (1) (2013) 62–67.

[55] W. Xu et al., Dielectric loaded graphene plasmon waveguide, Opt. Express 23 (4) (2015) 5147–5153.

[56] J. Zhu, J. Cheng, L. Zhang, Q.H. Liu, Modeling of 2D graphene material for plasmonic hybrid waveguide with enhanced near-infrared modulation, Mater. Lett. 186 (2017) 53–56.

[57] R. Rudrapati, "Graphene: Fabrication Methods, Properties, and Applications in Modern Industries," in Graphene Production and Application: IntechOpen Rijeka, 2020, pp. 9-22.

[58] M. Yang et al., Self-sustained solid-state exothermic reaction for scalable graphene production, Mater. Des. 196 (2020) 109135.

[59] J. Gong, H. Tang, M. Wang, X. Lin, K. Wang, J. Liu, Novel three-dimensional graphene nanomesh prepared by facile electro-etching for improved electroanalytical performance for small biomolecules, Mater. Des. 215 (2022) 110506.

[60] A. Lalbakhsh, R.B. Simorangkir, N. Bayat-Makou, A.A. Kishk, K.P. Esselle, Advancements and artificial intelligence approaches in antennas for environmental sensing, in: Artificial Intelligence and Data Science in Environmental Sensing, 2022, pp. 19–38.

[61] S. Adibi, M. A. Honarvar, and A. Lalbakhsh, "Gain enhancement of wideband circularly polarized UWB antenna using FSS," Radio Science, vol. 56, no. 1, pp. e2020RS007098-e2020RS007098, 2021.

[62] P. Das, K. Mandal, A. Lalbakhsh, Beam-steering of microstrip antenna using single-layer FSS based phase-shifting surface, Int. J. RF Microwave Comput. Aided Eng. 32 (3) (2022) e23033.

[63] J.M. Jornet, I.F. Akyildiz, Graphene-based plasmonic nano-antenna for terahertz band communication in nanonetworks, IEEE J. Sel. Areas Commun. 31 (12) (2013) 685–694.

[64] R. Degl'Innocenti et al., "Graphene-based optical modulator realized in metamaterial split-ring resonators operating in the THz frequency range," in Terahertz, RF, Millimeter, and Submillimeter-Wave Technology and Applications VII, 2014, vol. 8985: International Society for Optics and Photonics, p. 89851E.

[65] X. Zhao, C. Yuan, L. Zhu, J. Yao, Graphene-based tunable terahertz plasmon-induced transparency metamaterial, Nanoscale 8 (33) (2016) 15273–15280.

[66] A. Radwan, M. D'Amico, J. Din, G. G. Gentili, and V. Verri, "Bandwidth and gain enhancement of a graphene-based metamaterial antenna for the THz band," 2016.

[67] X. Huang et al., "Graphene metamaterials array based reconfigurable antenna," in 2016 International Symposium on Antennas and Propagation (ISAP), 2016: IEEE, pp. 106-107.

[68] A.A. Abdel Aziz, A.A. Ibrahim, M.A. Abdalla, Tunable array Antenna with CRLH feeding network based on graphene, IETE Journal of Research (2019) 1–9.

[69] S.H. Zainud-Deen, A.M. Mabrouk, H. Malhat, in: IEEE, 2017, pp. 1–4.

[70] M.U. Afzal, K.P. Esselle, A. Lalbakhsh, A Methodology to Design a Low-Profile Composite-Dielectric Phase-Correcting Structure, IEEE Antennas Wirel. Propag. Lett. 17 (7) (2018) 1223–1227, https://doi.org/10.1109/LAWP.2018.2840087.

[71] M. U. Afzal, K. P. Esselle, and A. Lalbakhsh, "A Metasurface to Focus Antenna Beam at Offset Angle," in 2018 2nd URSI Atlantic Radio Science Meeting (AT-RASC), 28 May-1 June 2018 2018, pp. 1-4, doi: 10.23919/URSI-AT-RASC.2018.8471483.

[72] M.U. Afzal, L. Matekovits, K.P. Esselle, A. Lalbakhsh, Beam-Scanning Antenna Based on Near-Electric Field Phase Transformation and Refraction of Electromagnetic Wave Through Dielectric Structures, IEEE Access 8 (2020) 199242–199253.

[73] A. Lalbakhsh, M.U. Afzal, K.P. Esselle, S.L. Smith, Wideband Near-Field Correction of a Fabry-Perot Resonator Antenna, IEEE Trans. Antennas Propag. 67 (3) (2019) 1975–1980, https://doi.org/10.1109/TAP.2019.2891230.

[74] A. Lalbakhsh, M.U. Afzal, K.P. Esselle, S.L. Smith, Low-Cost Nonuniform Metallic Lattice for Rectifying Aperture Near-Field of Electromagnetic Bandgap Resonator Antennas, IEEE Trans. Antennas Propag. 68 (5) (2020) 3328–3335, https://doi.org/10.1109/TAP.2020.2969888.

[75] S. Jarchi, Radiation pattern direction control of THz antenna with applying planar graphene metasurface, Optik (2021) 167458.

[76] M. Esfandiyari, S. Jarchi, M. Ghaffari-Miab, Channel capacity enhancement by adjustable graphene-based MIMO antenna in THz band, Opt. Quant. Electron. 51 (5) (2019) 1–11.

[77] Y. Luo et al., A graphene-based tunable negative refractive index metamaterial and its application in dynamic beam-tilting terahertz antenna, Microwave Opt. Technol. Lett. 61 (12) (2019) 2766–2772.

[78] Y.-J. Yang, B. Wu, Y.-T. Zhao, Dual-band beam steering THz antenna using active frequency selective surface based on graphene, EPJ Appl. Metamater. 8 (2021) 12.

[79] B. Wu, Y. Hu, Y.T. Zhao, W.B. Lu, W. Zhang, Large angle beam steering THz antenna using active frequency selective surface based on hybrid graphene-gold structure, Opt. Express 26 (12) (2018) 15353–15361.

[80] M. Gao, K. Li, F. Kong, H. Zhuang, and G. Zhu, "Graphene-Based Composite Right/Left-Handed Leaky-Wave Antenna at Terahertz," *Plasmonics,* vol. 15, no. 4, 2020.

[81] A. Lalbakhsh, M.U. Afzal, K.P. Esselle, S.L. Smith, All-Metal Wideband Frequency-Selective Surface Bandpass Filter for TE and TM polarizations, IEEE Trans. Antennas Propag. 70 (2022).

[82] Y. Cheng, J. Wang, Tunable terahertz circular polarization convertor based on graphene metamaterial, Diam. Relat. Mater. 119 (2021) 108559.

[83] S. Quader, J. Zhang, M.R. Akram, W. Zhu, Graphene-based high-efficiency broadband tunable linear-to-circular polarization converter for terahertz waves, IEEE J. Sel. Top. Quantum Electron. 26 (5) (2020) 1–8.

[84] Y. Wang, Y. Wang, Q. Li, Y. Zhang, S. Yan, C. Wang, Tunable graphene-based metasurface for an ultra-low sidelobe terahertz phased array antenna, Opt. Express 29 (17) (2021) 26865–26875.

[85] A. Lalbakhsh, M.U. Afzal, T. Hayat, K.P. Esselle, K. Mandal, All-metal wideband metasurface for near-field transformation of medium-to-high gain electromagnetic sources, Sci. Rep. 11 (1) (2021) 9421, https://doi.org/10.1038/s41598-021-88547-3.

[86] A. Lalbakhsh, M.U. Afzal, K.P. Esselle, S.L. Smith, All-Metal Wideband Frequency-Selective Surface Bandpass Filter for TE and TM polarizations, IEEE Trans. Antennas Propag. (2022).

[87] F. Parandin, N. Mahtabi, Design of an ultra-compact and high-contrast ratio all-optical NOR gate, Opt. Quant. Electron. 53 (12) (2021) 1–9.

[88] A. Vahdati, F. Parandin, Antenna patch design using a photonic crystal substrate at a frequency of 1.6 THz, Wireless Pers. Commun. 109 (4) (2019) 2213–2219.

[89] M. Abdollahi, F. Parandin, A novel structure for realization of an all-optical, one-bit half-adder based on 2D photonic crystals, J. Comput. Electron. 18 (4) (2019) 1416–1422.

[90] H. Saghaei, A. Zahedi, R. Karimzadeh, F. Parandin, Line defects on As2Se3-Chalcogenide photonic crystals for the design of all-optical power splitters and digital logic gates, Superlattices Microstruct. 110 (2017) 133–138.

[91] A. Lalbakhsh et al., A Compact C-Band Bandpass Filter with an Adjustable Dual-Band Suitable for Satellite Communication Systems, Electronics 9 (7) (2020) 1088.

[92] A. Ahmadi, S. V. Makki, A. Lalbakhsh, and S. Majidifar, "A novel dual-mode wideband band pass filter," *Applied Computational Electromagnetics Society Journal (ACES Journal),* vol. 29, no. 9, pp. 735–742-735–742, 2014.

[93] W. Qian, W. Xia, W. Zhou, R. Song, X. Zhao, D. He, A Graphene-Based Stopband FSS with Suppressed Mutual Coupling in Dielectric Resonator Antennas, Materials 14 (6) (2021) 1490.

[94] B. Zhang, J.M. Jornet, I.F. Akyildiz, Z.P. Wu, Mutual coupling reduction for ultra-dense multi-band plasmonic nano-antenna arrays using graphene-based frequency selective surface, IEEE Access 7 (2019) 33214–33225.

[95] Y. Shi, Y. Zhang, Generation of wideband tunable orbital angular momentum vortex waves using graphene metamaterial reflectarray, IEEE Access 6 (2017) 5341–5347.

[96] Z.K. Meng, Y. Shi, W.Y. Wei, Y. Zhang, L. Li, Graphene-based metamaterial transmitarray antenna design for the generation of tunable orbital angular momentum vortex electromagnetic waves, Optical Materials Express 9 (9) (2019) 3709–3716.

[97] S.H. Zainud-Deen, A.M. Mabrouk, H.-A.-E.-A. Malhat, Terahertz graphene based metamaterial transmitarray, Wireless Pers. Commun. 100 (3) (2018) 1235–1248.

[98] R. Mishra, R. Panwar, D. Singh, Equivalent circuit model for the design of frequency-selective, terahertz-band, graphene-based metamaterial absorbers, IEEE Magn. Lett. 9 (2018) 1–5.

[99] Q. Zhou et al., Graphene based controllable broadband terahertz metamaterial absorber with transmission band, Materials 11 (12) (2018) 2409.

[100] P. Fu, F. Liu, G.J. Ren, F. Su, D. Li, J.Q. Yao, A broadband metamaterial absorber based on multi-layer graphene in the terahertz region, Opt. Commun. 417 (2018) 62–66.

[101] J. Han, R. Chen, Tunable broadband terahertz absorber based on a single-layer graphene metasurface, Opt. Express 28 (20) (2020) 30289–30298, https://doi.org/10.1364/OE.403631.

[102] Y. Qi et al., "A Tunable Terahertz Metamaterial Absorber Composed of Hourglass-Shaped Graphene Arrays," *Nanomaterials,* vol. 10, no. 3, p. 533, 2020. [Online]. Available: https://www.mdpi.com/2079-4991/10/3/533.

[103] H. Zhang, F. Ling, H. Wang, Y. Zhang, B. Zhang, A water hybrid graphene metamaterial absorber with broadband absorption, Opt. Commun. 463 (2020) 125394.

[104] Q. Zou, Y. Shen, J. Ou-Yang, Y. Zhang, C. Jin, Polarization-insensitive graphene photodetectors enhanced by a broadband metamaterial absorber, Opt. Express 29 (15) (2021) 24255–24263, https://doi.org/10.1364/OE.433347.

[105] X. Du et al., A polarization- and angle-insensitive broadband tunable metamaterial absorber using patterned graphene resonators in the terahertz band, Opt. Laser Technol. 132 (2020), https://doi.org/10.1016/j.optlastec.2020.106513 106513.

[106] F. Chen, Y. Cheng, and H. Luo, "A Broadband Tunable Terahertz Metamaterial Absorber Based on Single-Layer Complementary Gammadion-Shaped Graphene," *Materials,* vol. 13, no. 4, p. 860, 2020. [Online]. Available: https://www.mdpi.com/1996-1944/13/4/860.

[107] Y. Chen, X. Pan, Z. Bao, Y. Wang, Z.-D. Hu, J. Wang, Tunable Terahertz Perfect-Absorbers With Dual Peak Based on Reverse Graphene Patch Metamaterials, IEEE Photonics J. 13 (3) (2021) 1–12.

[108] P. Jain et al., Graphene-based tunable multi-band metamaterial polarization-insensitive absorber for terahertz applications, J. Mater. Sci.: Mater. Electron. 31 (14) (2020) 11878–11886.

[109] S.K. Patel, V. Sorathiya, Z. Sbeah, S. Lavadiya, T.K. Nguyen, V. Dhasarathan, Graphene-based tunable infrared multi band absorber, Opt. Commun. 474 (2020) 126109.

[110] J. Bai, W. Shen, J. Shi, W. Xu, S. Zhang, and S. Chang, "A Non-Volatile Tunable Terahertz Metamaterial Absorber Using Graphene Floating Gate," *Micromachines,* vol. 12, no. 3, p. 333, 2021. [Online]. Available: https://www.mdpi.com/2072-666X/12/3/333.

[111] R. Jadeja et al., Numerical investigation of graphene-based efficient and broadband metasurface for terahertz solar absorber, J. Mater. Sci. 55 (8) (2020) 3462–3469, https://doi.org/10.1007/s10853-019-04269-y.

[112] M. Pan et al., Theoretical design of a triple-band perfect metamaterial absorber based on graphene with wide-angle insensitivity, Results Phys. 23 (2021), https://doi.org/10.1016/j.rinp.2021.104037 104037.

[113] J. Zhu, C. Wu, Y. Ren, Broadband terahertz metamaterial absorber based on graphene resonators with perfect absorption, Results Phys. 26 (2021), https://doi.org/10.1016/j.rinp.2021.104466 104466.

[114] T. Aghaee, A.A. Orouji, Reconfigurable multi-band, graphene-based THz absorber: Circuit model approach, Results Phys. 16 (2020), https://doi.org/10.1016/j.rinp.2019.102855 102855.

[115] A. Ghajar, A. Keshtkar, S. Jarchi, H. Ghorbaninejad, Genetic algorithm design for nonperiodic planar graphene leaky-wave antennas in THz, Int. J. RF Microwave Comput. Aided Eng. 32 (1) (2022) e22925.

[116] A. Lalbakhsh, M.U. Afzal, K.P. Esselle, Multiobjective particle swarm optimization to design a time-delay equalizer metasurface for an electromagnetic band-gap resonator antenna, IEEE Antennas Wirel. Propag. Lett. 16 (2016) 912–915.

[117] A. Lalbakhsh, M. U. Afzal, K. P. Esselle, and S. Smith, "Design of an artificial magnetic conductor surface using an evolutionary algorithm," in *2017 International Conference on Electromagnetics in Advanced Applications (ICEAA),* 2017: IEEE, pp. 885-887.

[118] A. Lalbakhsh, M.U. Afzal, B.A. Zeb, K.P. Esselle, "Design of a Dielectric Phase-Correcting Structure for an EBG Resonator Antenna Using Particle Swarm Optimization," in *Proc,* Int. Symp. Antennas Propag, Hobart, Australia, 2015.

[119] G. Roshani, E. Nazemi, M. Roshani, Usage of two transmitted detectors with optimized orientation in order to three phase flow metering, Measurement 100 (2017) 122–130.

[120] E. Nazemi, G. Roshani, S. Feghhi, S. Setayeshi, E.E. Zadeh, A. Fatehi, Optimization of a method for identifying the flow regime and measuring void fraction in a broad beam gamma-ray attenuation technique, Int. J. Hydrogen Energy 41 (18) (2016) 7438–7444.

[121] M. Roshani et al., Evaluation of flow pattern recognition and void fraction measurement in two phase flow independent of oil pipeline's scale layer thickness, Alexandria Eng. J. 60 (1) (2021) 1955–1966.

[122] A. Karami, G.H. Roshani, E. Nazemi, S. Roshani, Enhancing the performance of a dual-energy gamma ray based three-phase flow meter with the help of grey wolf optimization algorithm, Flow Meas. Instrum. 64 (2018) 164–172.

[123] G. Roshani, R. Hanus, A. Khazaei, M. Zych, E. Nazemi, V. Mosorov, Density and velocity determination for single-phase flow based on radiotracer technique and neural networks, Flow Meas. Instrum. 61 (2018) 9–14.

[124] M. Roshani et al., Combination of X-ray tube and GMDH neural network as a nondestructive and potential technique for measuring characteristics of gas-oil–water three phase flows, Measurement 168 (2021) 108427.

[125] M. Roshani et al., Application of GMDH neural network technique to improve measuring precision of a simplified photon attenuation based two-phase flowmeter, Flow Meas. Instrum. 75 (2020) 101804.

[126] M.A. Sattari et al., Applicability of time-domain feature extraction methods and artificial intelligence in two-phase flow meters based on gamma-ray absorption technique, Measurement 168 (2021) 108474.

[127] G. Roshani, E. Nazemi, Intelligent densitometry of petroleum products in stratified regime of two phase flows using gamma ray and neural network, Flow Meas. Instrum. 58 (2017) 6–11.

[128] G. Roshani, E. Nazemi, S. Feghhi, S. Setayeshi, Flow regime identification and void fraction prediction in two-phase flows based on gamma ray attenuation, Measurement 62 (2015) 25–32.

[129] G. Roshani, S. Feghhi, A. Mahmoudi-Aznaveh, E. Nazemi, A. Adineh-Vand, Precise volume fraction prediction in oil–water–gas multiphase flows by means of gamma-ray attenuation and artificial neural networks using one detector, Measurement 51 (2014) 34–41.

[130] G.H. Roshani et al., Online measuring density of oil products in annular regime of gas-liquid two phase flows, Measurement 129 (2018) 296–301.

[131] G. Roshani, E. Nazemi, S. Feghhi, Investigation of using 60Co source and one detector for determining the flow regime and void fraction in gas–liquid two-phase flows, Flow Meas. Instrum. 50 (2016) 73–79.

[132] G. Roshani, E. Nazemi, M. Roshani, Intelligent recognition of gas-oil-water three-phase flow regime and determination of volume fraction using radial basis function, Flow Meas. Instrum. 54 (2017) 39–45.

[133] P. Lalbakhsh, B. Zaeri, A. Lalbakhsh, M.N. Fesharaki, in: July. AntNet with reward-penalty reinforcement learning, In 2010 2nd International Conference on Computational Intelligence, Communication Systems and Networks, IEEE, 2010, pp. 17–21.

[134] H. Ahmadi, S. Vaezi, V.J. Harzand, R. Safian, Graphene-based terahertz metamaterial absorber for broadband applications, Solid State Commun. 323 (2021), https://doi.org/10.1016/j.ssc.2020.114023 114023.

[135] B.M. Karambasti, M. Ghodrat, G. Ghorbani, A. Lalbakhsh, M. Behnia, Design methodology and multi-objective optimization of small-scale power-water production based on integration of Stirling engine and multi-effect evaporation desalination system, Desalination 526 (2022) 115542.

[136] M. Soltani, A. Najafi, I. Chaharmahali, S. Biabanifard, A configurable two-layer four-bias graphene-based THz absorber, J. Comput. Electron. 19 (2) (2020) 719–735, https://doi.org/10.1007/s10825-020-01462-0.

[137] Y. Jia, H. Yin, H. Yao, J. Wang, C. Fan, Realization of multi-band perfect absorber in graphene based metal-insulator-metal metamaterials, Results Phys. 25 (2021), https://doi.org/10.1016/j.rinp.2021.104301 104301.

[138] J. Tian, R. Ke, R. Yang, W. Pei, Tunable quad-band perfect metamaterial absorber on the basis of monolayer graphene pattern and its sensing application, Results Phys. 26 (2021), https://doi.org/10.1016/j.rinp.2021.104447 104447.

[139] Z. Tang et al., Phosphorus science-oriented design and synthesis of multifunctional nanomaterials for biomedical applications, Matter 2 (2) (2020) 297–322.

[140] Y. Zhu et al., From phosphorus to phosphorene: Applications in disease theranostics, Coord. Chem. Rev. 446 (2021) 214110.

[141] Y. Wang et al., Emerging 2D material-based nanocarrier for cancer therapy beyond graphene, Coord. Chem. Rev. 400 (2019) 213041.

[142] M. Piliarik, L. Párová, J. Homola, High-throughput SPR sensor for food safety, Biosens. Bioelectron. 24 (5) (2009) 1399–1404, https://doi.org/10.1016/j.bios.2008.08.012.

[143] C. Zhang et al., U-bent fiber optic SPR sensor based on graphene/AgNPs, Sens. Actuators, B 251 (2017) 127–133, https://doi.org/10.1016/j.snb.2017.05.045.

[144] X. Zhou, X. Li, T. Cheng, S. Li, G. An, Graphene enhanced optical fiber SPR sensor for liquid concentration measurement, Opt. Fiber Technol. 43 (2018) 62–66, https://doi.org/10.1016/j.yofte.2018.04.007.

[145] Z. Xie et al., Black phosphorus-based photothermal therapy with aCD47-mediated immune checkpoint blockade for enhanced cancer immunotherapy, Light Sci. Appl. 9 (1) (2020) 1–15.

[146] S. Chen et al., "Eradication of tumor growth by delivering novel photothermal selenium-coated tellurium nanoheterojunctions," Science advances, vol. 6, no. 15, p. eaay6825, 2020.

[147] F. Yin et al., Black phosphorus quantum dot based novel siRNA delivery systems in human pluripotent teratoma PA-1 cells, J. Mater. Chem. B 5 (27) (2017) 5433–5440.

[148] P. Wan et al., Flexible transparent films based on nanocomposite networks of polyaniline and carbon nanotubes for high-performance gas sensing, Small 11 (40) (2015) 5409–5415.

[149] S. Yang et al., High sensitivity and good selectivity of ultralong MoO3 nanobelts for trimethylamine gas, Sens. Actuators, B 226 (2016) 478–485.

[150] T. Xue et al., Ultrasensitive detection of microRNA using a bismuthene-enabled fluorescence quenching biosensor, Chem. Commun. 56 (51) (2020) 7041–7044.

[151] D. Tyagi et al., Recent advances in two-dimensional-material-based sensing technology toward health and environmental monitoring applications, Nanoscale 12 (6) (2020) 3535–3559.

[152] M. Papi, "Graphene-Based Materials: Biological and Biomedical Applications," vol. 22, ed: Multidisciplinary Digital Publishing Institute, 2021, p. 672.

[153] A. Mazinani et al., Graphene oxide (GO) decorated on multi-structured porous titania fabricated by plasma electrolytic oxidation (PEO) for enhanced antibacterial performance, Mater. Des. 200 (2021) 109443.

[154] M.A. Shathi, M. Chen, N.A. Khoso, M.T. Rahman, B. Bhattacharjee, Graphene coated textile based highly flexible and washable sports bra for human health monitoring, Mater. Des. 193 (2020) 108792.

[155] Y. Chen, J. Ren, Y. Sun, W. Liu, X. Lu, S. Guan, Efficacy of graphene nanosheets on the plasma sprayed hydroxyapatite coating: Improved strength,

[156] F. Catania et al., A review on recent advancements of graphene and graphene-related materials in biological applications, Applied Sciences 11 (2) (2021) 614.

[157] C. Hu et al., A universally dispersible graphene-based ink modifier facilitates 3D printing of multi-functional tissue-engineered scaffolds, Mater. Des. 216 (2022) 110551.

[158] J. Li, X. Liu, J.M. Crook, G.G. Wallace, A 3D printed graphene electrode device for enhanced and scalable stem cell culture, osteoinduction and tissue building, Mater. Des. 201 (2021) 109473.

[159] J. Gao et al., Altered immune cells in the liver and spleen of mice as a typical immune response to graphene oxide exposure, Mater. Des. 206 (2021) 109802.

[160] X. Guo, H. Hu, X. Zhu, X. Yang, Q. Dai, "Higher order Fano graphene metamaterials for nanoscale optical sensing," (in eng), Nanoscale 9 (39) (2017) 14998–15004, https://doi.org/10.1039/c7nr05919a.

[161] A. Keshavarz, A. Zakery, Ultrahigh sensitive temperature sensor based on graphene-semiconductor metamaterial, Appl. Phys. A 123 (12) (2017) 797, https://doi.org/10.1007/s00339-017-1399-y.

[162] A.K. Sharma, A. Dominic, Influence of Chemical Potential on Graphene-Based SPR Sensor's Performance, IEEE Photonics Technol. Lett. 30 (1) (2018) 95–98, https://doi.org/10.1109/LPT.2017.2776945.

[163] X. Chen, W. Fan, C. Song, Multiple plasmonic resonance excitations on graphene metamaterials for ultrasensitive terahertz sensing, Carbon 133 (2018) 416–422, https://doi.org/10.1016/j.carbon.2018.03.051.

[164] S.-H. Lee et al., Graphene assisted terahertz metamaterials for sensitive bio-sensing, Sens. Actuators, B 310 (2020), https://doi.org/10.1016/j.snb.2020.127841 127841.

[165] M. Amin, M. Farhat, H. Bağcı, A dynamically reconfigurable Fano metamaterial through graphene tuning for switching and sensing applications, Sci. Rep. 3 (1) (2013) 2105, https://doi.org/10.1038/srep02105.

[166] Z. Yi et al., "Dual-Band Plasmonic Perfect Absorber Based on Graphene Metamaterials for Refractive Index Sensing Application," Micromachines, vol. 10, no. 7, p. 443, 2019. [Online]. Available: https://www.mdpi.com/2072-666X/10/7/443.

[167] D.B. Farmer, P. Avouris, Y. Li, T.F. Heinz, S.-J. Han, Ultrasensitive Plasmonic Detection of Molecules with Graphene, ACS Photonics 3 (4) (2016) 553–557, https://doi.org/10.1021/acsphotonics.6b00143.

[168] K. Li, X. Ma, Z. Zhang, J. Song, Y. Xu, G. Song, Sensitive refractive index sensing with tunable sensing range and good operation angle-polarization-tolerance using graphene concentric ring arrays, J. Physics D: Applied Physics 47 (40) (2014), https://doi.org/10.1088/0022-3727/47/40/405101 405101.

[169] W. Tang, L. Wang, X. Chen, C. Liu, A. Yu, W. Lu, "Dynamic metamaterial based on the graphene split ring high-Q Fano-resonnator for sensing applications," (in eng), Nanoscale 8 (33) (2016) 15196–15204, https://doi.org/10.1039/c6nr02321e.

[170] S. Xu et al., "Real-time reliable determination of binding kinetics of DNA hybridization using a multi-channel graphene biosensor, Nat. Commun. 8 (1) (2017/03/21 2017,) 14902, https://doi.org/10.1038/ncomms14902.

[171] W. Xu et al., Terahertz biosensing with a graphene-metamaterial heterostructure platform, Carbon 141 (2019) 247–252, https://doi.org/10.1016/j.carbon.2018.09.050.

[172] P.-R. Tang et al., Ultrasensitive specific terahertz sensor based on tunable plasmon induced transparency of a graphene micro-ribbon array structure, Opt. Express 26 (23) (2018) 30655–30666, https://doi.org/10.1364/OE.26.030655.

[173] H. Xu et al., Sensing analysis based on tunable Fano resonance in terahertz graphene-layered metamaterials, J. Appl. Phys. 123 (20) (2018) 203103.

[174] M.S. Islam et al., Tunable localized surface plasmon graphene metasurface for multiband superabsorption and terahertz sensing, Carbon 158 (2020) 559–567, https://doi.org/10.1016/j.carbon.2019.11.026.

[175] J. Huang et al., High sensitivity refractive index sensing with good angle and polarization tolerance using elliptical nanodisk graphene metamaterials, Phys. Scr. 94 (8) (2019) 085805.

[176] S. Gong, B. Xiao, L. Xiao, S. Tong, S. Xiao, X. Wang, Hybridization-induced dual-band tunable graphene metamaterials for sensing, Optical Materials Express 9 (1) (2019) 35–43, https://doi.org/10.1364/OME.9.000035.

[177] Y. Wang, Y. Wang, Z. Ji, W. Liang, W. Chen, Sensitive chemical potential sensor based on graphene hyperbolic metamaterials, EPL (Europhysics Letters) 130 (2) (2020) 27002.

[178] A. Hamouleh-Alipour, A. Mir, A. Farmani, Analytical Modeling and Design of a Graphene Metasurface Sensor for Thermo-Optical Detection of Terahertz Plasmons, IEEE Sens. J. 21 (4) (2021) 4525–4532, https://doi.org/10.1109/JSEN.2020.3035577.

[179] X. Du et al., Thermally-stable graphene metamaterial absorber with excellent tunability for high-performance refractive index sensing in the terahertz band, Opt. Laser Technol. 144 (2021), https://doi.org/10.1016/j.optlastec.2021.107409 107409.

[180] Y. Qi et al., A tunable terahertz metamaterial absorber composed of elliptical ring graphene arrays with refractive index sensing application, Results Phys. 16 (2020), https://doi.org/10.1016/j.rinp.2020.103012 103012.

[181] M. Farrokhfar, S. Jarchi, A. Keshtkar, Planar metamaterial sensor with graphene elliptical rings in transmission mode, Appl. Opt. 60 (8) (2021) 2434–2440, https://doi.org/10.1364/AO.418041.